Journal of Metals, Materials and Minerals, 35(1), e2196, 2025

Analyse the mechanical property optimization for FDM/3D-printed polycarbonate using Taguchi and TOPSIS techniques

N. SRINIVASA RAO[1], Raman KUMAR[2,3], N. KAVITHA[4], Ramachandran T[5], Hari Prasadarao PYDI[6], Aman SHANKHYAN[7], Ram SUBBIAH[8,*], Vikasdeep Singh MANN[9]

[1] *Department of Mechanical Engineering, Shri Vishnu Engineering College for Women, Bhimavaram, India*
[2] *University School of Mechanical Engineering, Rayat Bahra University, Kharar, Punjab 140103, India*
[3] *Faculty of Engineering, Sohar University, PO Box 44, Sohar, PCI 311, Oman*
[4] *Department of Physics, NPR College of Engineering and Technology, Natham, Dindigul 624401, Tamilnadu, India*
[5] *Department of Mechanical Engineering, School of Engineering and Technology, JAIN (Deemed to be University), Bangalore, Karnataka, India*
[6] *Department of Mechanical Engineering, College of Engineering and Technology, Bule Hora University, Ethiopia*
[7] *Centre for Research Impact & Outcome, Chitkara University Institute of Engineering and Technology, Chitkara University, Rajpura, 140401, Punjab, India*
[8] *Department of Mechanical engineering, Gokaraju Rangaraju Institute of Engineering and Technology, Nizampet Road, Bachupally, Kukatpally Hyderabad, 500090, Telangana State, India*
[9] *Department of Mechanical Engineering, Chandigarh Engineering College, Chandigarh Group of Colleges-Jhanjeri, Mohali140307, Punjab, India*

***Corresponding author e-mail**: ram4msrm1@gmail.com

Received date:
6 November 2024
Revised date:
3 December 2024
Accepted date:
23 December 2024

Keywords:
FDM;
3D printing;
Optimization;
UTS;
CMS

Abstract

Fused Deposition Modeling is 3D printing techniques which chiefly appreciated for prototypes. This manufacturing process works by extrusion of thermoplastic materials to make the three-dimensional objects. In this work, we pursued to identify the FDM parameters to increase mechanical properties, specifically ultimate tensile strength (UTS) and compressive strength (CMS). Polycarbonate was chosen to create the test samples because of the best thermal and mechanical properties, which was the increasing manufacturing applications of 3D printing. Nine experiments were conducted to verify the interaction of the considered parameters, namely infill rate (IR), printing speed (PS), and film height (FH). The combined use of the Taguchi and TOPSIS approaches makes the interaction of the considered parameters clearer, pointing out the most favorable combinations in terms of optimizing the mechanical properties of 3D-printed polycarbonate samples. From the Taguchi-TOPSIS method results, the optimal parameters were acknowledged as IR1-PS1-FH2. An experiment focused under these optimal settings resulted in UTS of 29.59 MPa and CMS of 34.5 MPa. Furthermore, the relative closeness coefficients for the initial and optimized factors were 0.36182 and 0.7734 respectively, proving a significant improvement in product quality. Finally, this study highlighted the potential for further refinement of FDM processes in enhancing the mechanical properties, provided the valuable insights for industries leveraging additive manufacturing for high-performance applications.

1. Introduction

3D printing was the advanced technology which emerged for making 3Dimensional products. It also helps in the advantages of products like making flexible products, doesn't require molding, especially small productions, and prototype requirements. Process Beginning with the design of a component that was selected through the use of CAD software; this 3D model can be transformed into a Stereolithography file to make it compatible with the 3D printers. [1]. Representative 3D printers were equipped with print head which moved along the x, y, and z axis, permitting precise deposition of materials according to the model. these printers could work with a variation of materials such as plastics, metals , and biological materials [2]. FDM Factors such as infill density, layer thickness, nozzle temperature, and raster angle all play a crucial role in finding the final quality of the printed parts [3,4]. Most of the researches were dedicated to optimizing the FDM factors for various 3D printing technologies and explored the relationship between factors and the mechanical properties of printed parts, concentrating on enhancing surface finish, dimensional accuracy, and minimizing material wastages [5-8]. Gohil *et al.* [9] printed some test samples of the photopolymer resin at 365 nm with a DLP 3D printer to check the prospect of this resin. The author used some parameters: time it takes for the print, layer thickness, and exposure time that all made up some vital parameters to get a good quality 3D printing material.The findings indicated that the DLP printer maintained a superior degree of precision while

also being economically advantageous relative to existing options. Lefkothea Antonara *et al.* [10] utilized FDM- 3D printing technology to streamline the production of microneedles by directly preparing negative molds. The optimized 3D-printed molds were employed to make microneedle arrays using polyvinyl alcohols (PVA)/polyvinyl pyrrolidone (PVP) matrix, with Galantamine hydrobromide as API. A detailed analysis showed that the PVA, drug load, and their interaction had great impact on controlling the release profile of Galantamine. This method proposal several advantage such as reduced manufacturing complexity and enlarged control over drug release, making it a promising technique for future applications. M. Saravana Kumar *et al.* [11] studied the processing defects in 3D printing and CRITIC method embedded within the WASPAS framework is employed. PLA specimens were printed for both flexural and tensile testing. The parametric significance analysis revealed that layer thickness, printing speed, and temperature play a critical role in controlling the strength and quality of the printed objects and also Mathematical optimizations based on composite established that optimal results were achieved with a layer thickness of 0.1 mm, printing speed of 60 $mm \cdot s^{-1}$, and temperature of 200°C. the Validation experiments established the yielding flexural strength of 78.52 MPa, UTS of 45.52 MPa, and impact strength of 6.21 $kJ \cdot m^{-2}$. Zaman *et al.* [12] investigated the effects of FDM on the mechanical strength of parts produced by 3D printers. The results clearly identified infill percentage as the most critical factor influencing the overall strength of the printed parts. A higher infill percentage contributed to greater internal density, thereby enhancing the load-bearing capacity and durability of the printed objects. Hussein Alzyod *et al.* [13] employed a numerical approach to explore the correlation between residual stress and three parameters. The numerical analysis exposed that printing orientation exerted the most substantial effect on the residual stress within the printed parts. Adjusting the orientation of the print could alter how stress was distributed and accumulated during the cooling and solidification of layers.Abeykoon *et al*. [1] investigated 3D printing parameters on the mechanical properties of printed parts, with Polylactic Acid (PLA). Their study exposed that filling density played a great role in improving the elastic modulus of components. Precisely, PLA parts with 100% filling density showed remarkable elastic modulus of 1538 MPa which indicate the good strength that achieved through higher internal material density. Habibur Rahman *et al.* [14] examined the impact of six key process parameters of FDM. The experimental results discovered that measured dimensions in the Z-direction were larger than the CAD model, while dimensions in the X and Y directions were minor. The % of deviations for each axis were calculated, along with surface roughness and to optimize these multi-response outcomes, GRA was applied. Based on the findings, appropriate scale factors for each direction were determined and used to adjust the CAD dimensions to correct for the observed dimensional deviations. Anis Bahar *et al.* [15] used Polycarbonate (PC) as a capable material for these insulators due to its fire resistance and the stability of its physical properties at high temperatures. The result indicated that printing temperature of 280°C is optimal for achieving superior tensile strength. Furthermore, the study reveals that as the infill rate increases, both thermal conductivity and thermal effusively improve, while thermal diffusivity tends to decrease. Nectarios Vidakis *et al.* [16]developed nanocomposites using PC with the addition of CNF at concentrations of 0.5 wt% and 1.0 wt%. Mechanical tests were performed to evaluate the efficacy of the composites. Additionally, SEM was employed to obtain pictures of the specimen's peripheral surfaces and fracture region. The findings demonstrated that the incorporation of 0.5 wt% CNF yielded superior mechanical performance relative to both PC and the 1.0 wt% PC CNF nanocomposite. Xun Chen *et al*. [17] Utilized an orthogonal test combined with the TOPSIS entropy weight optimization theory, an optimization approach for the preparation of CFRPF/PC. The findings indicated that the diameter performance index has the greatest weight, about 0.75, highlighting overall quality assessment. The optimal parameters for making CCFRPF/PC were found to be mold temperature of 285°C, temperature of 305°C, and speed of 1 $m \cdot min^{-1}$. the resulting properties achieved included diameter of 0.375 mm, roundness of 29.4 μm, curvature radius of 9.775 mm, and UTS of 1298 MPa. Giovanni Gómez-Gras *et al*. [18] presented characterization of PC-ISO, concentrating on printing parameters in Fused Filament Fabrication affect the mechanical properties. Based on the findings, optimal combinations of printing parameters for applications in biomechanics are suggested. Additionally, the study highlighted the necessity of combining PC-ISO with other materials to achieve the mechanical strengths required for effective bone platform.

Based on the above literature studies, it was detected that no researches have been done on 3D printing samples using polycarbonate material to evaluate their mechanical properties such as the ultimate tensile strength and compressive strength as per ASTM standards. A combined approach of the Taguchi and TOPSIS methods employed to analyse the interactions among selected factors, allowing identification of the most favourable combinations for optimizing the mechanical performance of the 3D-printed polycarbonate samples.

2. Materials selection and methods

This research concentrated on polycarbonate as the principal material owing to its extensive application across several sectors. The selection of polycarbonate is justified by its superior mechanical qualities and resilience. The L9 orthogonal array was selected to denote nine experimental runs [19]. This methodology arranges tests in a defined order to assess the influence of each parameter, guaranteeing that data from each iteration facilitates a comprehensive study of results. To create samples using the FDM process (Figure 1(a)), each CATIA file was first converted to the STL file format [20,21]. The STL format was compatible with a wide range of software applications and extensively used in computer-aided manufacturing and 3D printing. After designing the tensile, and compressive testing specimens as per ASTM standards in CATIA, the blueprint was transferred in STL format by changing the file extensions from .cat to stl. The overall workflow of this process was illustrated in Figure 1(b).

To evaluate tensile properties, ASTM D638 specimens were used. UTS represented the maximum force applied before fracture, divided by the sample cross-sectional area. Figure 2-3 illustrate UTS specimens before and after testing. For compressive testing, ASTM D695 specimens were used to assess compressive strength. CMS was calculated using the formula $F = P/A$, where F is the compressive strength in MPa, P is the maximum applied force in newtons, and A is the initial area in mm^2. Figure 4-5 show the CMS specimens before and after compression testing, respectively.

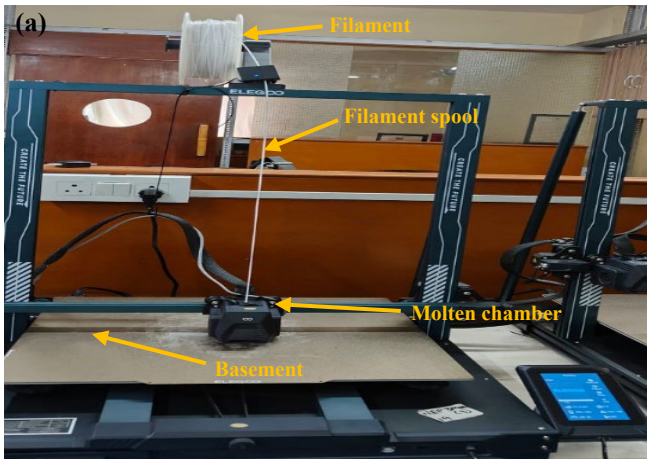

Figure 1. (a) FDM process, and (b) Flow process of this work.

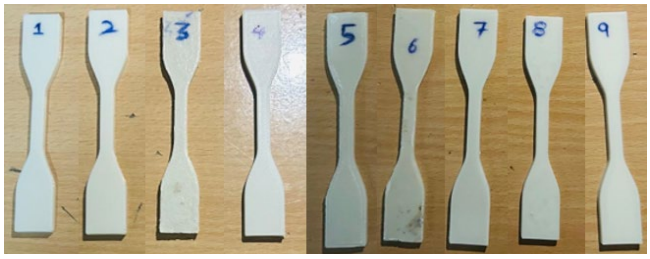

Figure 2. Tensile test samples.

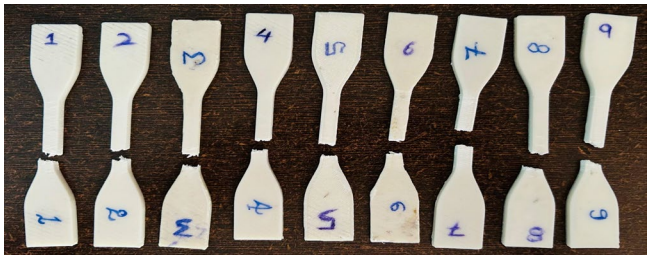

Figure 3. Broken sample of Tensile test.

Figure 4. Compressive test samples.

Figure 5. Samples after compressive test.

2.1 Taguchi and TOPSIS method

The Taguchi technique utilises an L9 orthogonal array design, a systematic matrix with rows and columns, where each column represents distinct factors or circumstances that fluctuate throughout experiments. By applying the Taguchi method, a streamlined approach to optimizing quality and performance is achieved, significantly reducing the number of required experiments [22]. The orthogonal array allows for comprehensive analysis of the interactions among process parameters. Taguchi's procedure uses the S/N ratio to improve the performance characteristics. Typically, the S/N ratio can be characterized into two categories: the lower-the-better (Equation (1)), the larger-the-better (Equation (2)).

$$SN_{\text{Large}} = -10\log\left(\frac{1}{n}\sum_{i=1}^{n}\frac{1}{x_{ij}^2}\right) \quad (1)$$

The aim of this work was to maximize the UTS and CMS. Therefore, the 'larger the better' criterion was used for UTS and CMS.

$$SN_{\text{Small}} = -10\log\left(\frac{1}{n}\sum_{i=1}^{n}x_{ij}^2\right) \quad (2)$$

TOPSIS is an efficient nonparametric approach, which has been used in a very wide range of cases for the determination of the best alternative from a set of alternatives. It is particularly suitable when there are several conflicting criteria. In this research, TOPSIS was applied to integrate three major responses, namely UTS and CMS into one composite performance measure. While applying this, the best alternative would be identified. There are six basic steps for the application of the TOPSIS method:

Step 1: Construct the decision matrix. Here, (i = 1,2,…,n) represents the number of alternatives, and (j = 1,2,…,q) denotes the criteria. The matrix entries reflect the performance values of each criterion (i) associated with alternative (j). This matrix forms the foundation for subsequent analysis in Equation (3-4).

$$\text{Decision matrix} = \begin{bmatrix} x_{11} & x_{12} & \dots & x_{1z} \\ x_{21} & x_{22} & \dots & x_{2z} \\ \dots & \dots & \dots & \dots \\ x_{n1} & x_{n2} & \dots & x_{nz} \end{bmatrix} \quad (3)$$

$$T_{ij} = \frac{z_{ij}}{\sqrt{\sum_{i=1}^{n} z_{ij}^2}} \quad (4)$$

Step 2: ND is needed due to all the criteria have units or scales. It converts raw data into unitless numbers so that criteria are comparable. Normalization of each element in the decision matrix is done by dividing it with the Euclidean norm.

Step 3: Develop the weighted decision matrix (WM) in Equation (5). Assign weights to each response to reflect their relative importance in the decision-making process. In this study, equal weights of 0.25 are allotted to TS, HN, and WR, indicating that each response is considered equally significant.

$$\text{weighted decision matrix (WM)} = u_{ij} = W_i t_{ij} \quad (5)$$

Step 4: Find the positive ideal solution (PIS) and the negative ideal solution (NIS). The PIS represented the scenario where the benefit criteria were maximized Contrarywise, the NIS reflected a situation where the benefit criteria are minimized and the cost criteria were maximized. These ideal solutions have given reference points for evaluating the alternatives.

$$c^+ = (c_1^+, c_2^+, \ldots, c_n^+) \text{ for max values}$$

$$c^- = (c_1^-, c_2^-, \ldots, c_n^-) \text{ for min values}$$

Step 5: Calculate the separation measures. The parting from the PIS (V+) and NIS (V−) were computed using Euclidean distance. These measures quantify how far each alternative was from the ideal and worst-case scenarios respectively using Equation (6-7).

$$V_i^+ = \sqrt{\sum_{j=1}^{N} \left(C_{ij} - C_j^+\right)^2} \quad (6)$$

$$V_i^- = \sqrt{\sum_{j=1}^{N} \left(C_{ij} - C_j^-\right)^2} \quad (7)$$

Step 6: Calculate the relative closeness coefficient, CCi. The more significant its value, the closer the alternative to the ideal solution. Equations of calculated CCi are used to rank the options available. Equation (8) identifies the preferred solution as the alternative with the highest CCi. Table 8 shows the final TOPSIS results.

$$CC_i = \frac{V_i^-}{V_i^+ + V_i^-} \quad (8)$$

3. Result and discussion

3.1 The interaction plots on UTS

The interaction plots among the parameters for UTS are shown in Figure 6-8. Figure 6 reveal that the interaction plot between PS and IR demonstrates a positive effect on the UTS. This indicates that UTS increases with higher IR and lower PS. With a higher infill rate, the structure of the material can better distribute the applied loads across the part. More interconnected material in the infill allows more continuous paths through which the stress could distribute without causing local failure in case tensile stresses occur. The outcome from interaction between FH and IR resulting from graph in Figure that UTS increases as a result of an increase in the value of FH and IR (Figure 7). More significant bonding between individual layers could occur for a thicker film or layer. Thicker layers tend to bond well when deposited, and the fewer possible weak points at interfaces of layers the greater the tensile strength is likely to be, because material tends to act cohesively under tension. Figure 6 reveal that the interaction plot between PS and FH demonstrates effect on the UTS. This indicates that UTS increases with higher FH and lower PS. At slower speeds, the extrusion of material tends to be more consistent and uniform.

Table 1. Process factors with levels.

Factors	Level 1	Level 2	Level 3
Infill rate (IR)	80%	90%	100%
Printing speed (PS)	50 mm·s^{-1}	60 mm·s^{-1}	70 mm·s^{-1}
Film height (FH)	0.15 mm	0.20 mm	0.25 mm

Table 2. UTS and CMS results.

Infill rate, IR [%]	Printing speed (PS) [mm·s^{-1}]	Film height, FH [mm]	Ultimate tensile strength, UTS [MPa]	Compressive strength, CMS [MPa]
80	50	0.15	21.11	28.19
80	60	0.2	24.27	30.01
80	70	0.25	19.67	31.342
90	50	0.2	28.53	42.158
90	60	0.25	26.91	42.012
90	70	0.15	22.45	41.699
100	50	0.25	38.1	49.682
100	60	0.15	35.35	52.421
100	70	0.2	36.16	53.823

Table 3. S/N ratio for UTS.

Level	Infill rate (IR)	Printing speed (PS)	Film height (FH)
1	-26.69	-29.07	-28.16
2	-28.24	-29.09	-29.32
3	-31.25	-28.02	-28.70
Delta	4.56	1.07	1.16
Rank	1	3	2

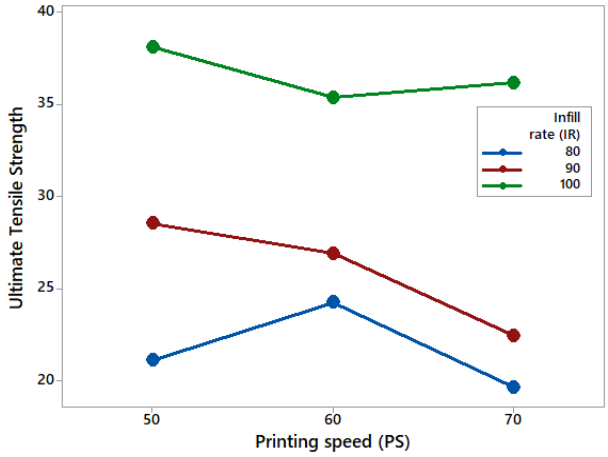

Figure 6. IR vs PS on UTS.

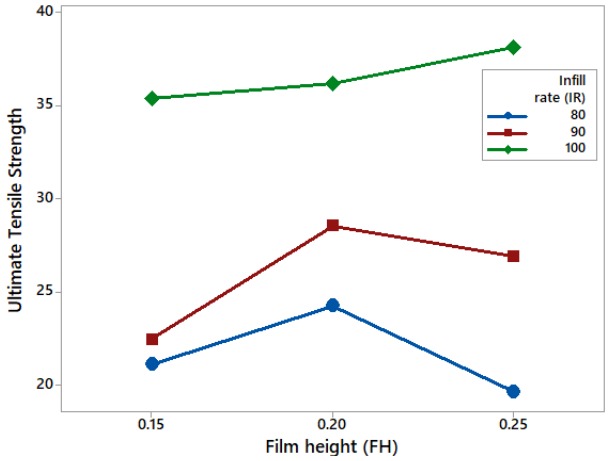

Figure 7. IR vs FH on UTS.

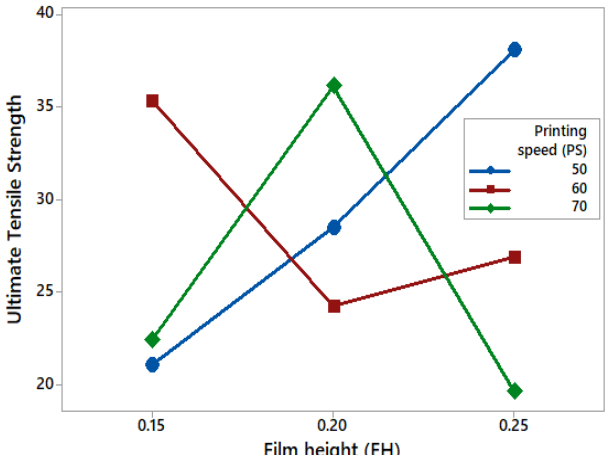

Figure 8. FH vs PS on UTS.

3.2 Analysis of variance (ANOVA)

The ANOVA tables for S/N ratio are presented for UTS and CMS in Table 4 and Table 6 respectively. The F-test was to evaluate the importance of process parameters, where the high F-value suggested that a factor has a substantial effect on the process response [24,26-28]. In this work, the infill rate emerged as the most influencing factor (98.1%), contributing to both UTS and CMS. The p-value for the infill rate is less than 0.05, indicating that this parameter has a statistically significant influence on tensile strength at a 95% confidence level. Amongst the various factors analysed, the infill rate had the highest impact, contributed 88.2% to UTS and 98.1% to CMS. From this, the infill rate's pivotal role in optimizing both mechanical properties, as it ensured highest material density and improved layer bonds and the film height had the smallest effect on CMS and UTS. Despite its lower contribution, film height still played role in finding the overall material performance. This analysis highlighted that optimizing infill rate was essential for improving UTS and CMS in 3D printed materials.

3.3 The interaction plots on CMS

The interaction charts for the parameters affecting UTS are presented in Figures 10-12. Figure 10 illustrates that the interaction plot between PS and IR exhibits a beneficial impact on the CMS. This signifies that CMS rises with an IR of 100% and a PS of 50 mm·s^{-1}. An elevated IR guarantees a more significant accumulation of material within a specified duration. This results in a denser and more regular arrangement of powder particles, which, during processing, yields fewer voids and enhanced bonding among particles.

Improved density directly correlates to enhanced compressive strength and A lower PS, which translates to slower spreading of powder, allows for more consistent layering. Each layer gets adequate time to settle and bond well with the previous layer, reducing porosity. This finer control over layer thickness helps in achieving a more compact and stronger material.

The interaction outcome between FH and PS, as resulting from the graph which shows that CMS increases with increasing FH of 70 mm and PS of 50 mm·s^{-1} (Figure 11). Increasing film height decreases the number of layers used for part construction. A reduced number of layers results in diminished chances for defects to arise at the interfaces, such voids, insufficient bonding, or layer misalignments. The decrease in flaws enhances overall strength, especially under compressive loads where material density and uniformity are essential.

Figure 12 illustrates that the interaction plot between IR and FH influences the CMS. This signifies that CMS rises with an increased FH of 0.2 mm and an IR of 100%. At moderate FH values, the material can flow and distribute more uniformly between layers, hence diminishing the likelihood of porosity, partial melting, or unbonded areas. Layers that are either too thin or overly thick may create additional voids or weak points, hence diminishing compressive strength. The 0.2 mm thickness achieves equilibrium, resulting in a consistent structure with reduced imperfections.

3.4 SN ratio

The Signal-to-Noise (SN) ratio in experimental design, especially within the Taguchi technique, aims to measure performance variance caused by noise components and to determine ideal circumstances that reduce variability and improve the robustness of experimental data [29-33]. The signal-to-noise ratio aids in identifying configurations that optimise ultimate tensile strength and compressive strength while reducing the effects of external factors or inaccuracies [25]. Figure 9's S/N ratio plots and the data in Table 3 indicate that the ideal parameters

for maximising ultimate tensile strength are an infill rate of 100%, a print speed of 60 mm·s^{-1}, and a layer height of 0.2 mm. These conditions facilitate optimal adhesion between the layers, hence improving tensile performance by minimising voids and flaws during the printing process. Figure 13 and Table 5 indicate that optimal conditions for enhancing compressive strength are associated with an infill rate of 100%, accompanied by a somewhat elevated print speed of 70 mm·s^{-1} and an identical film height of 0.2 mm. The increased print speed in this instance may enhance layer adhesion under compressive stresses, while the uniform infill rate and film height guarantee a dense and consistent structure. This combination offers maximal resistance to deformation under compressive forces.

Table 4. Analysis of variance for UTS.

Source	DF	Seq SS	Adj MS	F	P	%
IR	2	32.2634	16.1317	1136.48	0.001	88.2
PS	2	2.2419	1.1209	78.97	0.013	6.12
FH	2	2.0342	1.0171	71.65	0.014	5.48
Residual Error	2	0.0284	0.0142			0.2
Total	8	36.5678				

Table 5. S/N ration for CMS.

Level	Infill rate (IR)	Printing speed (PS)	Film height (FH)
1	-29.49	-31.81	-31.93
2	-32.46	-32.13	-32.22
3	-34.31	-32.31	-32.10
Delta	4.82	0.51	0.29
Rank	1	2	3

Table 6. Analysis of Variance for CMS.

Source	DF	Seq SS	Adj MS	F	P	%
IR	2	35.4832	17.7416	220.50	0.005	98.1
PS	2	0.3962	0.1981	2.46	0.289	1.09
FH	2	0.1271	0.0636	0.79	0.559	0.35
Residual Error	2	0.1609	0.0805			0.46
Total	8	36.1674				

Table 7 Normalized and Weighted Normalized values for TOPSIS.

Exp. no	Normalized		Weighted normalized	
	UTS	CMS	UTS	CMS
1	0.244206	0.238039	0.085472	0.083314
2	0.280762	0.213832	0.098267	0.074841
3	0.227548	0.218404	0.079642	0.076441
4	0.330043	0.226742	0.115515	0.07936
5	0.311302	0.211411	0.108956	0.073994
6	0.311302	0.243418	0.108956	0.085196
7	0.440751	0.229432	0.154263	0.080301
8	0.408938	0.227549	0.143128	0.079642
9	0.418308	0.213832	0.146408	0.074841

Table 8. Positive ideal solution readings.

Exp. no	Difference square for V+		Sum square for V+	V+
	UTS	CMS		
1	4.77342E-07	2.21497E-05	0.085472	0.083314
2	0.000146497	0.000173681	0.098267	0.074841
3	4.25274E-05	0.000134064	0.079642	0.076441
4	0.000861533	7.50008E-05	0.115515	0.07936
5	0.000519506	0.000196733	0.108956	0.073994
6	0.000519506	7.97328E-06	0.108956	0.085196
7	0.004637578	5.95799E-05	0.154263	0.080301
8	0.003245047	7.01884E-05	0.143128	0.079642
9	0.00362945	0.000173681	0.146408	0.074841

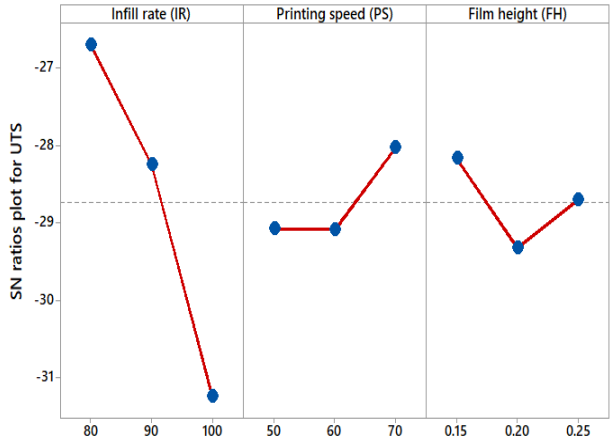

Figure 9. S/N ratio plot for UTS.

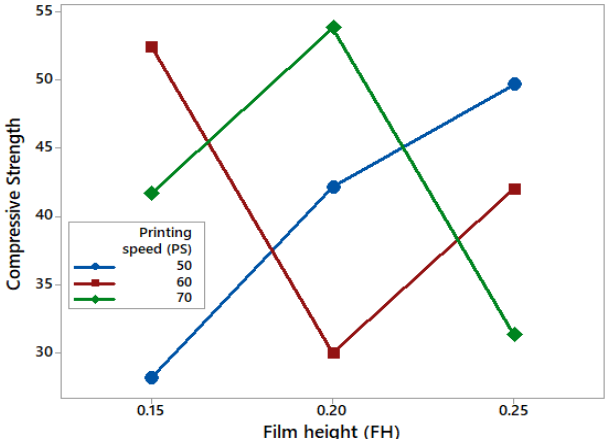

Figure 11. FH vs PS on CMS.

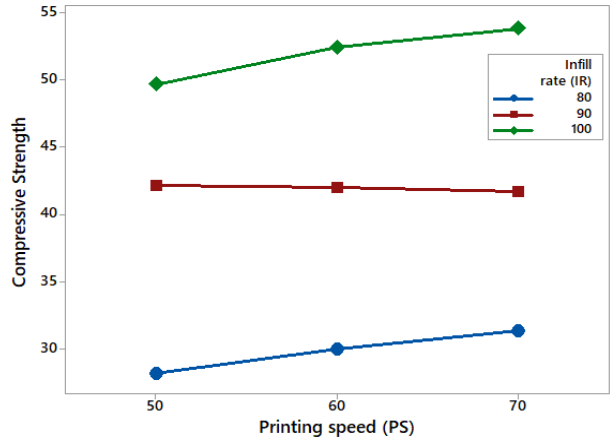

Figure 10. IR vs PS on CMS.

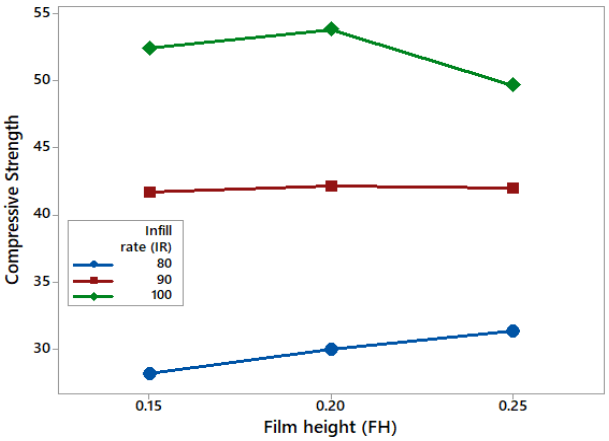

Figure 12. IR vs FH on CMS.

Table 9. Negative ideal solution readings.

Exp. no	Difference square for V–		Sum square for V–	V–
	UTS	CMS		
1	0.012511	0.010356	0.000264	0.01624
2	0.025306	0.001883	0.000644	0.02538
3	0.006681	0.003483	5.68E-05	0.00753
4	0.042554	0.006402	0.001852	0.04303
5	0.035995	0.001036	0.001297	0.03601
6	0.035995	0.012238	0.001445	0.03802
7	0.081302	0.007343	0.006664	0.08163
8	0.070167	0.006684	0.004968	0.07048
9	0.073447	0.001883	0.005398	0.07347

Table 10. Relative closeness Coefficient.

Exp. no	Relative closeness (CCi)	Rank
1	0.77346	1
2	0.58646	3
3	0.36182	9
4	0.58440	4
5	0.57365	5
6	0.62340	2
7	0.54361	8
8	0.55039	6
9	0.54366	7

Table 11. Confirmation test result.

	Initial parameters	Optimal parameters	
		Prediction	Experiment
Level	**IR1-PS3-FH3**	**IR1-PS1-FH2**	**IR1-PS1-FH2**
Ultimate Tensile strength (MPa)	19.67	-	29.59
Compressive Strength (MPa)	31.342	-	34.5
Relative Closeness coefficient	0.36182	0.77346	-

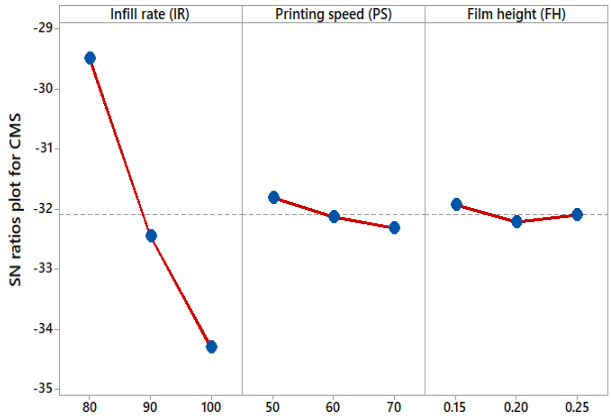

Figure 13. S/N ratio plot for CMS.

3.5 Confirmation test result

After determining the optimal parameters, a confirmation trial is conducted to validate the optimized results. Equation (7) is used to predict the optimal values for UTS and CMS. This trial serves as a final check to ensure that the predicted improvements in mechanical properties are achieved under the selected optimal conditions. By comparing the experimental results with the predicted values, the effectiveness of the optimization process can be confirmed, providing confidence in the reliability of the model and the chosen parameters.

$$¥ = ¥_j + \sum_{i=1}^{n} \left(¥_i - ¥_j\right) \quad (7)$$

where $¥_j$ represents the overall closeness coefficient value, n is the number of controlled factors, and $¥_i$ is the closeness coefficient at the optimal condition. With help of Taguchi-TOPSIS method, The optimal parameter combination was recognized as IR1-PS1-FH2. under these optimal conditions, the yielded the following results: UTS of 29.59 MPa, CMS of 34.5 MPa. CCi for the initial and optimized process parameters were 0.36182 and 0.77346 respectively. Table 10 conceded the calculated values for the initial and optimal runs. The observed improvement in the predilection value for the ideal solution was 0.4116. Therefore, the results of the confirmation test demonstrated the successful optimization of the process which validating the effectiveness of the Taguchi-TOPSIS method.

4. Conclusion

This research aimed to optimize the FDM process factors to improve the UTS and CMS of 3D-printed polycarbonate samples. The combination of the Taguchi method and TOPSIS was employed for optimization. The key conclusions were discussed below:

- From the Taguchi S/N Ratio Analysis, The optimal parameters for achieving the highest UTS were determined to be an infill rate of 100%, a print speed of 60 mm·s^{-1}, and a film height of 0.2 mm. Likewise, the best conditions for maximizing CMS were also linked to a 100% infill rate but with a slightly higher print speed of 70 mm·s^{-1}, while maintaining the same film height of 0.2 mm.
- From the ANOVA Results, the infill rate was found to be the most significant, contributing 88.2% to UTS and an even higher 98.1% to CMS. In contrast, film height was the least influential factor, having a minimal effect on both UTS and CMS. While film height had the lowest impact, it still played a role in determining the overall mechanical performance of the material.
- From the Taguchi-TOPSIS Optimization result, the optimal combination of parameters was identified as IR1-PS1-FH2. An experiment conducted under these optimal conditions resulted in a UTS of 29.59 MPa and CMS of 34.5 MPa. Additionally, the relative closeness coefficients for the initial and optimized process parameters were 0.36182 and 0.77346, respectively, indicating a substantial improvement in mechanical performance.
- The results validate the effectiveness of the Taguchi-TOPSIS method in optimizing FDM process variables to significantly improve the tensile and compressive strength of 3D-printed polycarbonate samples.

References

[1] C. Abeykoon, P. Sri-Amphorn, and A. Fernando, "Optimization of fused deposition modeling parameters for improved PLA and ABS 3D printed structures," *International Journal of Lightweight Materials and Manufacture,* vol. 3, no. 3, pp. 284-297, 2020.

[2] E. Guerra, J. de Lara, A. Malizia, and P. Díaz, "Supporting user-oriented analysis for multi-view domain-specific visual languages," *Information and Software Technology*, vol. 51, no. 4, pp. 769–784, 2009.

[3] M. Shirmohammadi, S. J. Goushchi, and P. M. Keshtiban, "Optimization of 3D printing process parameters to minimize surface roughness with hybrid artificial neural network model and particle swarm algorithm," *Progress in Additive Manufacturing*, vol. 6, no. 2, pp. 199-215, 2021.

[4] A. M. Chugay, and A. V. Zhuravka, "Packing optimization problems and their application in 3D printing," *Advances in Computer Science for Engineering and Education III*, pp. 75-85. 2021.

[5] T. Peng, "Analysis of energy utilization in 3D printing processes," *Procedia CIRP*, vol. 40, pp. 62-67, 2016.

[6] M. Elbadawi, A. W. Basit, and S. Gaisford, "Energy consumption and carbon footprint of 3D printing in pharmaceutical manufacture," *International Journal of Pharmaceutics*, vol. 639, p. 122926, 2023.

[7] I. Gibson, D. Rosen, and B. Stucker, Additive Manufacturing Technologies. New York, NY: Springer New York, 2015.

[8] S. Ramadan, Q. Altwarah, M. Abu-Shams, and D. Alkurdi, "Optimizing tensile strength and energy consumption for FDM through mixed-integer nonlinear multi-objective optimization and design of experiments," *Heliyon*, vol. 10, no. 9, p. e30164, 2024.

[9] J. Gohil, R. Gohil, R. Gundaraniya, M. Prajapati, and S. Fefar, "Design and fabrication of DLP 3D printer," *Engineering, Materials Science*, pp. 283-292, 2020.

[10] L. Antonara, P. P. Dallas, and D. M. Rekkas, "A novel 3D printing enabled method for fast and reliable construction of polymeric microneedles using experimental design," *Journal of Drug Delivery Science and Technology*, vol. 68, p. 102888, 2022.

[11] M. S. Kumar, M. U. Farooq, N. S. Ross, C.-H. Yang, V. Kavimani, and A. A. Adediran, "Achieving effective interlayer bonding of PLA parts during the material extrusion process with enhanced mechanical properties," *Scientific Reports*, vol. 13, no. 1, p. 6800, 2023.

[12] U. K. uz Zaman, E. Boesch, A. Siadat, M. Rivette, and A. A. Baqai, "Impact of fused deposition modeling (FDM) process parameters on strength of built parts using Taguchi's design of experiments," I*nternational Journal of Advanced Manufacturing Technology*, vol. 101, no. 5-8, pp. 1215-1226, 2019.

[13] H. Alzyod, L. Borbas, and P. Ficzere, "Rapid prediction and optimization of the impact of printing parameters on the residual stress of FDM-ABS parts using L27 orthogonal array design and FEA," *Materials Today: Proceedings*, vol. 93, pp. 583-588, 2023.

[14] H. Rahman, T. D. John, M. Sivadasan, and N. K. Singh, "Investigation on the scale factor applicable to ABS based FDM additive manufacturing," *Materials Today: Proceedings*, vol. 5, no. 1, pp. 1640-1648, 2018.

[15] A. Bahar, S. Belhabib, S. Guessasma, F. Benmahiddine, A. E. A. Hamami, and R. Belarbi, "Mechanical and thermal properties of 3D printed polycarbonate," Energies, vol. 15, no. 10, p. 3686, 2022.

[16] N. Vidakis, M. Petousis, E. velidakis, M. spiridaki, and J. D. kechagias, "mechanical performance of fused filament fabricated and 3D-printed polycarbonate polymer and polycarbonate/ cellulose nanofiber nanocomposites," *Fibers*, vol. 9, no. 11, p. 74, 2021.

[17] X. Chen, Y. Wang, M. Liu, S. Qu, Q. Zhang, and S. Chen, "Preparation and process parameter optimization of continuous carbon fiber-reinforced polycarbonate prepreg filament," *Polymers (Basel)*, vol. 15, no. 3, p. 607, 2023.

[18] G. Gómez-Gras, M. D. Abad, and M. A. Pérez, "Mechanical performance of 3D-printed biocompatible polycarbonate for biomechanical applications," *Polymers (Basel)*, vol. 13, no. 21, p. 3669, 2021.

[19] B. Srinivas, P. Satishkumar, R. Saminathan, and B. Srikanth, "Optimization of process parameters in 3D printing of polycarbonate for high heat applications," *Interactions*, vol. 245, no. 1, p. 119, 2024.

[20] B. Uhrich, M. Schäfer, O. Theile, and E. Rahm, "Using physics-informed machine learning to optimize 3D printing processes," *Progress in Digital and Physical Manufacturing*, pp. 206-221, 2023.

[21] B. Ramos, D. Pinho, D. Martins, A. I. F. Vaz, and L. N. Vicente, "Optimal 3D printing of complex objects in a 5–axis printer," *Optimization and Engineering*, vol. 23, no. 5, pp. 1085-1116, 2022.

[22] P. Awasthi, A. Kumar, P. M. Pandey, and S. S. Banerjee, "Optimization of process parameters of 3D printed thermoplastic elastomeric materials using statistical modeling with particular reference to mechanical properties and print quality," *Functional Composite Materials*, vol. 5, no. 1, p. 6, 2024.

[23] D. K. Pratiwi, A. Arifin, Gunawan, A. Mardhi, and Afriansyah, "Investigation of welding parameters of dissimilar weld of SS316 and ASTM A36 joint using a grey-based taguchi optimization approach," *Journal of Manufacturing and Materials Processing*, vol. 7, no. 1, p. 39, 2023.

[24] T. T. Nguyen, V. H. Hoang, V.-T. Nguyen, and V. T. T. Nguyen, "Dissimilar MIG welding optimization of C20 and SUS201 by taguchi method," *Journal of Manufacturing and Materials Processing*, vol. 8, no. 5, p. 219, 2024.

[25] S. Ahmed, R. A. ur Rahman, A. Awan, S. Ahmad, W. Akram, M. Amjad, M. Y. Yahya, and S. S. R. Koloor, "Optimization of process parameters in friction stir welding of aluminum 5451 in marine applications," *Journal of Marine Science and Engineering*, vol. 10, no. 10, p. 1539, 2022.

[26] K. Doungkeaw, P. Suttipong, P. Kungwankrai, S. Muengto, B. Thavornyutikarn, and J. Tungtrongpairoj, "Recycling of iron oxide waste by carbothermic reduction to utilize in FDM 3D printing materials," J*ournal of Metals, Materials and Minerals*, vol. 33, no. 2, pp. 156-161, 29, 2023.

[27] A. Khosravi, M. Randjbar, And R. Habibpour, "Synthesis, characterization, and application of ZIF-8 for removal of Cd, Ni, and Pb ions from aqueous solutions: Optimization of the process by Response Surface Methodology (RSM) based on Central Composite Design (CCD) technique," *Journal of Metals, Materials and Minerals*, vol. 33, no. 2, pp. 88-102, 2023.

[28] P. Seensattayawong, C. Suwanpreecha, N. Boonlert, S. Songkuea, and A. Manonukul, "The effect of printing parameters on the properties of 17-4 PH stainless steel fabricated by material extrusion additive manufacturing," *Journal of Metals, Materials and Minerals*, vol. 34, no. 2, p. 1804, 2024.

[29] S. Vijayakumar, J. J. Kakkassery, J. Maniraj, P. S. Satheesh Kumar, M. Vignesh, and G. Anbuchezhiyan, "ANN modeling and optimization of friction stir welding performance for AA6061 and AA5083 alloy joints," *Proceedings of the Institution of Mechanical Engineers, Part E: Journal of Process Mechanical Engineering,* 2024.

[30] B. Venkatesh, R. Sivakumar, S. Vijayakumar, P. S. S. Kumar, M. N. S. Sri, and A. Pradeep, "Predict the modelling of cement

concrete strength using Taguchi and ANOVA method," *Interactions*, vol. 245, no. 1, 2024.

[31] P. S. Kumar, V. Rao, K. P. Indira, D. J. Rani, S. Vijayakumar, and R. Haranath, "Enhancement of TIG welding performance on carbon steel by Taguchi-TOPSIS optimization," *Interactions,* vol. 245, no. 1, pp. 1-11, 2024.

[32] S. Jeyakrishnan, S. Vijayakumar, M. N. S. Sri, and P. Anusha, "An integration of RSM and ANN modelling approach for prediction of FSW joint properties in AA7178/AA5456 alloys," C*anadian Metallurgical Quarterly*, pp. 1-18, 2024.

[33] B. Gugulothu, K. Bharadwaja, S. Vijayakumar, T. V. J. Rao, M. N. S. Sri, P. Anusha, and M. K. Agrawal, "Modeling and parametric optimization of electrical discharge machining on casted composite using central composite design," *International Journal on Interractive Design and Manufacturing*, vol. 18, pp. 2793-2803, 2024.

[34] P. Anusha, M. N. S. Sri, S. Vijayakumar, T. V. J. Rao, P. Paramasivam, S. Jeyakrishnan, and K. K. Saxena, "Design and optimization the wear characteristics for Al7178/TiO2/B4C/FA central hybrid composite," *International Journal on Interactive Design and Manufacturing*, vol. 18, no. 8, pp. 5773-5781, 2023.

[35] S. Karumuri, B. Haldar, A. Pradeep, S. A. K. Karanam, M. N. S. Sri, A. Peyyala, N. Sateesh, R. Subbian, and S. Vijayakumar, "Multi-objective optimization using Taguchi based grey relational analysis in friction stir welding for dissimilar aluminium alloy," *International Journal on Interactive Design and Manufacturing,* vol. 18, no. 3, pp. 1-18, 2023.